NATIONAL ADVISORY COMMITTEE FOR AERONAUTICS

TECHNICAL NOTE 2870

POWER-OFF FLARE-UP TESTS OF A MODEL HELICOPTER ROTOR IN VERTICAL AUTOROTATION

By S. E. Slaymaker and Robin B. Gray

Princeton University

Washington

January 1953

NATIONAL ADVISORY COMMITTEE FOR AERONAUTICS

TECHNICAL NOTE 2870

POWER-OFF FLARE-UP TESTS OF A MODEL HELICOPTER ROTOR IN VERTICAL AUTOROTATION

By S. E. Slaymaker and Robin B. Gray

SUMMARY

This report presents the results of an experimental investigation into the problem of reducing the descending velocity of a helicopter model in steady vertical autorotation by expending the kinetic energy of the rotor in a collective-pitch flare. Test data were obtained over a wide range of operating conditions from a freely falling model rotor restrained laterally by a guide wire. The results indicate the influence of disk loading and rotor inertia on a given rotor configuration under various flare conditions. All tests were made outside of ground effect.

An attempt was made to develop a semiempirical method of predicting the flare-up performance of the model, and the result is presented herein. The accuracy of this method was checked experimentally for all model configurations and sample calculations were made for several full-scale helicopters. The method yields results which compare favorably with experimental data.

INTRODUCTION

This work represents an attempt to investigate practical limitations in rate and amount of blade pitch change required to produce an effective flare-up with a given rotor configuration descending in steady vertical autorotation. It is generally known that flare performance may be improved by increasing rotor energy through heavier blades or higher tip speed and also by increasing rate and amount of blade pitch change in the flare. However, it seems desirable to know the manner in which these variables operate in order to be able to predict their effect on performance. For this purpose, these tests have been carried out on the model rotor system not only for practical values of the variables but also in ranges which would be disastrous in flight. For simplicity, the tests were limited to vertical flight.

This investigation was carried out at Princeton University under the sponsorship and with the financial assistance of the National Advisory Committee for Aeronautics.

SYMBOLS

Physical quantities:

W	gross weight of model, pounds
b	number of blades
R	blade radius, feet
S	rotor disk area, square feet
c	blade-section chord, feet
σ	rotor solidity ratio ($bc/\pi R$)
$\bar{\theta}$	average blade pitch angle from zero lift, three-quarter radius for twisted blades, radians unless otherwise stated
$\dot{\bar{\theta}}$	rate of change of average blade pitch angle, radians per second per second ($d\bar{\theta}/dt$)
$\bar{\theta}_f$	final blade pitch angle, radians unless otherwise stated
I_R	mass moment of inertia of rotor about center of rotation, slug-feet^2
I_l	mass moment of inertia of blade about center of rotation, slug-feet^2
γ_l	mass constant of rotor blades; expresses ratio of air forces to centrifugal forces ($c\rho aR^4/I_l$)
ρ	mass density of air, slugs per cubic foot
t	time, seconds
t_θ	length of blade-pitch-change cycle, seconds
g	acceleration due to gravity (32.2 ft/sec^2)

Velocities and accelerations:

V_V	vertical velocity, rate of descent positive downwards, feet per second
$\dot{V}_V$	rate of change of vertical velocity, feet per second per second

$V_{v_{auto}}$ steady rate of vertical autorotative descent, feet per second

$V_{v_{min}}$ minimum rate of descent during flare-up, feet per second

v average effective induced velocity at rotor (always positive), feet per second

u average rotor inflow velocity, feet per second $(V_v - v)$

Ω rotor angular velocity, radians per second

$\dot{\Omega}$ rate of change of rotor angular velocity, radians per second per second $(d\Omega/dt)$

Ω_{auto} rotor angular velocity in autorotation

Blade-section characteristics:

a slope of lift curve, per radian

c_{d_o} section profile-drag coefficient

$\delta_0, \delta_1, \delta_2$ coefficients in a power series for c_{d_o} as a function of angle of attack $\left(c_{d_o} = \delta_0 + \delta_1\bar{\alpha} + \delta_2\bar{\alpha}^2\right)$

$\bar{\alpha}$ average blade angle of attack, radians

Rotor characteristics:

$\bar{C}_L$ average rotor lift coefficient $\left(\bar{C}_{L_{basic}} + \Delta\bar{C}_L\right)$

$\bar{C}_{L_{basic}}$ average basic rotor lift coefficient (empirical)

$\Delta\bar{C}_L$ additional correction to $\bar{C}_{L_{basic}}\left(0.0126\,\frac{W}{S}\,\bar{\theta}_t + \frac{\dot{\bar{\theta}}_t}{\Omega_t}\right)$ ($\bar{\theta}_t$ and $\dot{\bar{\theta}}_t$ in deg)

T rotor thrust, pounds

F rotor thrust coefficient based on resultant velocity $\left(\frac{T}{2\pi\rho R^2 u^2}\right)$

f rotor thrust coefficient based on rate of descent $\left(\frac{T}{2\pi\rho R^2 V_v^2}\right)$

Subscripts:

o initial value

t value at time t

DESCRIPTION OF APPARATUS

The apparatus for this project consisted of an enclosed flight space, a model rotor system with associated driving mechansim, and various units of electrical equipment for making and recording the necessary measurements.

Tower

The necessary flight space was provided by a fully enclosed tower (fig. 1), free from cross winds, weather, and so forth, which allowed at least 1-rotor-diameter clearance about the model throughout its flight, in order to minimize interference effects. A control room above the flight chamber housed all drive-mechanism and data-recording equipment. The model could be raised into the control room to make necessary adjustments before each test. A guide wire down the center of the tower passed through the rotor axis to keep the fall of the model truly vertical and to prevent tilting of the rotor axis. There was no other restraint on the model while in flight. An accelerating device was provided at the starting position of the model in order to reduce the drop distance required for the model to reach a steady descending velocity. A shock absorber stopped the model at the bottom of the tower.

Model

The test model itself consisted of a two-bladed, controllable-pitch rotor system with the following characteristics:

Rotor diameter, ft	8
Solidity ratio	0.08
Blade section (no twist or taper)	NACA 0015
Dry weight (with light blades), lb	12.3

Two sets of blades were provided which differed only in weight. One set provided a total rotor inertia of 0.66 slug-feet^2, and the other set provided 1.25 slug-feet^2. Blades were installed (fig. 2) without drag hinges but were free to flap from -7° to 15°. Changes of blade pitch angle were made in flight up to 15°, governed by a hydraulic timing device which was adjustable for both amount and rate of pitch change. The pitch-change cycle was initiated by a second timing device which permitted the occurrence of the pitch change to be set for any desired time after the model was released. Figure 3 shows these hub mechanisms in section. Disk loading of the basic model was increased for various tests by addition of lead weights to the base of the hub.

Instrumentation

During a drop test, all data were taken by photoelectric pickup tubes with appropriate amplifying circuits and were recorded against time by a recording oscillograph. Vertical motion of the model was detected by a series of horizontal light beams and phototubes along the drop path. Rotor speed was counted by a vertical light beam through the rotor. A third phototube circuit recorded the starting time of the test and also the blade pitch angle during the pitch-change cycle of the flare. This was accomplished by means of a number of photoflash bulbs installed on the model with batteries and suitable contacts (fig. 4). The first bulb was flashed as the model was released to start its drop. A second bulb fired as the pitch-change cycle began, and subsequent bulbs flashed for each 2° of pitch change up to 10°. For changes greater than this, the resulting curve of pitch against time must be extrapolated.

Drive Mechanisms

The model drive system was operated by a 5-horsepower, direct-current motor with a Ward Leonard speed control which turned the drive shaft through a belt drive and spline coupling. (See fig. 5.) The model was held onto the lower end of the drive shaft by a manually operated release mechanism (fig. 6). To provide initial acceleration of the model, the drive shaft was arranged to move downwards about 4 feet, and extra accelerating force was applied to the shaft by a number of rubber shock cords. Solenoid-operated catches held the shaft on the driving spline and released the shaft and model at the same instant (fig. 5). Figure 7 shows the starting position of the model beneath the control-room floor. Figure 8 shows drive shaft in final position at the end of the acceleration stroke.

TEST PROCEDURE

Considerable preliminary work was done with the model before beginning actual tests of flare-ups. Basic rotor characteristics were determined by means of static-thrust tests on a model lift stand. The curve of minimum profile-drag coefficient against Reynolds number for this model is shown in figure 9. The lift stand used lacked sufficient power to obtain data at high angles of attack, but past experience with similar models has determined that, in the range of Reynolds numbers of these tests, the drag polar can be expressed as:

$$c_d = \left(c_{d_o}\right)_{min} + 0.9\bar{\alpha}^2$$

For each value of disk loading to be used in the flare tests, values of rotor speed and rate of descent in steady autorotation were determined experimentally. Autorotative rotor speed was determined by making a series of drops of the model at autorotative blade pitch, with different initial rotor speeds. Curves of rotor speed during these drops were plotted together, and the rotor speed toward which they tended to converge was taken as the autorotative value, and this was used for subsequent flare tests. Steady rate of descent in autorotation was determined from drops of the model at autorotative rotor speed without any flare. The amount of acceleration required to bring the model to full autorotative rate of descent within about the first 20 percent of the drop distance was determined by trial for each disk loading.

A typical flare test with given disk loading and rotor inertia was begun by setting the desired initial and final blade pitch angles and rate of pitch change. The delay timer was adjusted so that the flare occurred about halfway down the tower and the test results were therefore obtained in a region outside of ground effects. Flash bulbs were installed and the model was lowered to starting position at the end of the drive shaft. Sufficient shock cords were connected to the drive shaft to provide the needed initial acceleration, and the model was brought up to a speed slightly above autorotative rotor speed. Recording equipment was started before the model was released and it was kept running until the model hit the shock absorber at the bottom of the tower.

Tests were normally run in groups, with only one variable being changed in each group. Six rotor conditions were covered (two inertias and three disk loadings), and for each of these conditions at least two groups of tests were run. One group varied the amount of pitch change at a given rate, and the other varied the rate of pitch change with a given amount. Test data for each group were plotted together as curves

of displacement, rotor speed, and blade pitch angle against time. Curves of descending velocity against time were computed for each test.

Flare tests at disk loadings higher than 0.8 were not made because of damage to the test model.

PRECISION OF TEST RESULTS

By conservative estimate, time at any position could be read from the oscillograph record to the nearest 0.005 second, while position error of the phototubes has been determined by several measurements to be not over 3/32 inch. Based on this, the computed accuracy of the resulting velocity curve should be 4 percent or better. The accuracy of the rotor speed data was calculated at about 2 percent, based on an estimated time reading error of 0.003 second in 2 revolutions. Curves of blade pitch angle are believed to be accurate within $1/4^{\circ}$, as calibration has shown the contact spacing to be within these limits, and tests have shown that time lag in the flash-bulb signal is negligible.

RESULTS AND DISCUSSION

Justification of Initial Conditions

At the start of the test program, there was some question as to what autorotative blade angle was to be used, what autorotative rotor speed was to be used, and to what velocity the model should be accelerated. Previous tests on transition from hovering to autorotation (reference 1) had indicated that in the dropping distance available, higher "final" descending velocities were realized than were expected. At that time, it was not known whether these higher velocities were due to the descent of the model into its own wake or to a recirculation of air in the tower. To avoid any possibility of setting up a circulation in the tower while the model was being brought up to speed, it was decided to accelerate and drop the model with an initial blade angle of 0°.

Autorotative rotor speed was obtained by making a series of unaccelerated drops at different initial speed values for each rotor configuration. A typical series of curves is shown in figure 10. As may be seen from the figure, there is a definite convergence toward a steady rotor speed. This value was taken as the correct autorotative rotor speed for this particular rotor disk loading.

It was also found that a steady rate of descent was then obtained when the model was dropped at the autorotative rotor speed. The values so

obtained for all disk loadings are plotted in figure 11 on $1/f$ against $1/F$ coordinates. The results compare very favorably with the data of reference 2.

The effect of initial acceleration on autorotative velocity, rotor speed, and distance required to reach autorotation was investigated and the results for one configuration are shown in figure 12. It was found that the amount of acceleration was not too critical and the model rather quickly adjusted its rate of descent to a steady value after release from the accelerating device. In general, the effect of the initial acceleration on rotor speed was negligible.

Effect of Rate of Change of Blade Pitch Angle

The effects of varying the rate of change of blade pitch angle on displacement, rate of descent, and rotor speed for one disk loading and rotor inertia are shown in figure 13. The curve of $\bar{\theta}$ against time was parabolic so that, in general, the rate of change of blade pitch angle varies continuously throughout the pitch-change interval. In all cases the initial blade angle was set at 0° and the final blade angle was set at $12\frac{1}{2}^\circ$. The total pitch-change time t_θ covered the range of 0.22 second to 2.96 seconds.

As may be seen from figure 13, the effect of the rate of change of blade pitch angle on displacement and hence velocity is quite large as the total pitch-change time becomes small, the most pronounced effect occurring when t_θ is of the order of 1/2 second. It appears for this disk loading, however, that the major advantages of decreasing t_θ have been realized when t_θ is approximately 1/3 second. Further reductions in t_θ seem to yield smaller improvements in flare performance. Data for other disk loadings indicate that the value of t_θ at which the most pronounced effect occurs tends to decrease with increasing disk loading. At a disk loading of 0.855 pound per square foot this value of t_θ is of the order of 1/4 second. This is believed to be a definite trend even though the pitch-change-time curve had to be extrapolated for $\bar{\theta}_f > 10\frac{1}{2}^\circ$.

Within experimental error, the curves of rotor speed against time are essentially linear throughout the portion of the maneuver prior to minimum velocity, the slopes of the curves becoming more negative as the total pitch-change time decreased. The largest effect appeared between 2.96 seconds $> t_\theta >$ 1.44 seconds for a disk loading of 0.573 pound per square foot, the slope changing from -1.88 radians per second per second to -7.85 radians per second per second in this interval. For t_θ = 0.22 second, $\dot{\Omega}$ = -10.15 radians per second per second.

Effect of Final Blade Pitch Angle

The effect of varying the final blade pitch angle on displacement, rate of descent, and rotor speed for one disk loading and rotor inertia is shown in figure 14. The variation of t_θ with final blade pitch angle may be closely approximated by the formula

$$t_\theta = 0.99\left(\bar{\theta}_f\right)^{1.20}$$

In all cases, the initial blade angle was 0°.

As may be seen from figure 14, the final blade pitch angle has a remarkable effect on the minimum rate of descent. Changing the final angle from 11° to 12° results in a change in rate of descent from 8.7 feet per second to 1.2 feet per second. A blade pitch change to $12\frac{1}{2}^\circ$ yields a rate of ascent of 1.2 feet per second. It would then appear that the minimum rate of descent is very sensitive to final blade pitch angle, especially at minimum velocities near 0 feet per second and at low rates of descent. It is also apparent that, for the range covered, an increase in final blade angle yields a more successful flare maneuver. For $\bar{\theta}_f = 15^\circ$, the minimum velocity is a rate of ascent of 5.1 feet per second. However, in general, the effect of an increase in disk loading was to make the change in minimum velocity less sensitive to final blade pitch angle.

As in the previous case, the variation of rotor speed with time for various final blade pitch angles is essentially linear (within experimental error) for the disk loadings and inertias tested, with the slopes of the curves becoming more negative with increasing $\bar{\theta}_f$.

Effect of Rotor Inertia and Disk Loading

The effect of rotor inertia and disk loading on rate of descent and rotor speed is shown in figure 15. This figure shows that, for a given blade-pitch-angle variation, an increase in disk loading decreases the effectiveness of the flare maneuver, whereas an increase in rotor inertia increases the effectiveness. This, of course, is what might have been expected.

Except for one case, it would appear that, for a given rotor inertia, the change in rate of descent from autorotation to minimum flare velocity is approximately constant and therefore independent of disk loading. If this is true, it would seem to indicate that the minimum rate of descent

for the configuration with a disk loading of 0.246 pound per square foot and $\gamma_1 = 5.3$ should be about 1.5 feet per second instead of -4.0 feet per second. Further investigation showed that, for this particular case, the rotor speed had increased from 400 rpm to 430 rpm during the drop prior to the initiation of the flare maneuver. Other tests made at the same time of the same configuration did not show this increase so it must be assumed to be in error for some unknown reason. At the time of discovery of this error, it was impractical to repeat the test. The results, however, are included as a rough indication of the effect of initial rotor speed on the flare maneuver.

The data indicate that, in general, increasing disk loading and/or decreasing rotor inertia increases negatively the slope of the curve of rotor speed against time.

Figure 16 is a plot of the change in rate of descent from autorotation to minimum rate of descent divided by autorotative velocity against average rate of blade pitch change for all disk loadings, rotor inertias, and final blade pitch angles. Presented in this one figure are all the data taken during the entire investigation at the point of minimum rate of descent. In general, previous discussions hold throughout the complete range covered.

Semiempirical Theory

A semiempirical method of predicting the flare-up performance of the model is developed in appendix A. This method is based primarily on figure 17 which shows the empirical variation of the average basic rotor lift coefficient with blade pitch angle during flare-up from steady vertical autorotation. This curve was calculated from experimental data using equation (A1) of appendix A. In performing this calculation it was assumed that $\dot{\Omega}_t$ was a constant, that the pitch change was completed within the first interval of time (i.e., $t_\theta < 0.2$ sec), and that $\bar{C}_{L_{basic}}$ was a function only of blade pitch angle. The first two assumptions are shown to be good within experimental error by the experimental data (figs. 13, 14, and 15). The validity of the third assumption can only be indicated by the results of the method. Figure 18 shows the results of the calculations based on the above assumptions. As may be seen, the semiempirical curves agree quite well with experiment; the only appreciable error appears to lie in the fact that the time required to reach minimum velocity and hence altitude required for flare to be completed just at touch down cannot be predicted by these curves. The values of $\bar{C}_{L_t}$ which were determined by this calculation were corrected for $\bar{\theta}_t$ and disk loading according to equations (A2) and (A3) of appendix A and form the basis of figure 17.

Figures 19 and 20 present a true comparison of the semiempirical theory with experimental results. The only experimental data which were used were the physical characteristics of the model and the experimental curve of $\bar{\theta}$ against time. The figures show that the theory predicts the minimum rate of descent quite well for all disk loadings, total pitch-change times, and rotor inertias. The only exception is the configuration with a disk loading of 0.246 pound per square foot in figure 20. This exception has been previously discussed in the section "Effect of Rotor Inertia and Disk Loading." If the experimental minimum rate of descent should be of the order of 1.5 feet per second as previously supposed, then the theory also agrees quite well with this configuration.

The flare-up performance of two full-scale helicopters as predicted by this semiempirical method was calculated and the results are plotted in figure 21. To the authors' knowledge there are no experimental data available for comparison purposes.

A sample calculation has been included in appendix A to indicate the computational procedures.

CONCLUSIONS

Within the range of disk loadings and rotor inertias covered by this investigation of the flare-up performance of a model helicopter, the following conclusions may be drawn:

1. For a given disk loading and rotor inertia, an increase in rate of change of blade pitch angle and in amount of final blade pitch angle results in a more effective flare maneuver. There is some indication, however, that the major increases in performance are rather quickly realized and further increases yield a diminishing increase in results.

2. For a given rate of change of blade pitch angle and final blade pitch angle, an increase in rotor inertia for a given disk loading increases the effectiveness of the flare maneuver, whereas an increase in disk loading for a given rotor inertia decreases the effectiveness. In the latter case, the experimental data seem to indicate that the rotor is capable of reducing the rate of descent by a fixed amount which is dependent only on blade angle, rate of change of blade angle, and rotor inertia. Therefore, since the autorotative rate of descent increases with disk loading for a given configuration, the effectiveness of the flare should decrease by about the same amount.

3. The variation of rotor speed during the flare maneuver is essentially linear.

4. The semiempirical method for predicting the flare performance of a model helicopter rotor as developed herein yields accurate minimum rates of descent throughout the range of experimental investigation.

Princeton University
Princeton, N. J., April 17, 1952

APPENDIX A

DEVELOPMENT OF SEMIEMPIRICAL METHOD

The method of predicting the flare-up performance of a model helicopter in vertical autorotation as developed herein is no more than an attempt to correct a simple theory by the addition of empirical constants and by the neglect of apparently unimportant terms. In the beginning it had seemed feasible to assume that, as a first approximation, a flare-off landing could be considered as an inverse transition from hovering to autorotation and the theory of reference 3 would apply. This supposition was quickly shown to be erroneous, however, when an attempt was made to predict the flare velocities of the model rotor. For lack of another approach, it was decided to use the same basic method, namely, Newton's second law and the simple blade-element theory, to arrive at expressions for the rate of change of vertical velocity and the rate of change of angular velocity. The expressions could then be modified by the addition of empirical factors and neglect of terms so that they might be made to fit the experimental results.

Hence, by applying Newton's second law to the vertical motion of the model and by assuming an average rotor lift coefficient so that the expression for the rotor thrust as determined by blade-element theory may be integrated, the following expression is obtained:

$$\dot{V}_{v_t} = g - \frac{\sigma \bar{C}_{L_t} \rho (\pi R^2)(\Omega_t R)^2}{6(W/g)} \tag{A1}$$

Thus, in order that $\dot{V}_{v_t}$ and hence V_{v_t} may be determined, expressions must be found for the average rotor lift coefficient $\bar{C}_{L_t}$ and for the rotor angular velocity Ω_t.

It was then found by a series of trial-and-error computations that the average rotor lift coefficient could be empirically expressed as

$$\bar{C}_{L_t} = \bar{C}_{L_{basic_t}} + \Delta\bar{C}_{L_t} \tag{A2}$$

where $\bar{C}_{L_{basic_t}}$ is determined from the empirical curve of $\bar{C}_{L_{basic}}$ against $\bar{\theta}$ as shown in figure 17, and

$$\Delta\bar{C}_{L_t} = 0.0126 \frac{W}{S} \bar{\theta}_t + \frac{\dot{\bar{\theta}}_t}{\Omega_t} \qquad \left(\bar{\theta}_t \text{ and } \dot{\bar{\theta}}_t \text{ in deg}\right) \tag{A3}$$

is an empirically determined expression which introduces a correction depending upon disk loading, blade pitch angle, rate of change of blade pitch angle, and rotor angular velocity. (Note that dimensions are automatically accounted for by the empirical constants.)

In a manner similar to that used for equation (A1), an expression was arrived at for the rate of change of angular velocity. (See equation (13), reference 3.) It was found, however, that this expression, when used in its entirety, yielded results which did not compare well with experiment. Further computations and modifications yielded the following expression

$$\dot{\Omega}_t = - \frac{c\rho a R^4}{I_R} \left(\frac{\bar{\theta}_t \Omega_{auto}^2}{7420} + 1.1 \dot{\bar{\theta}}_t \right) \qquad \left(\bar{\theta}_t \text{ and } \dot{\bar{\theta}}_t \text{ in deg}\right) \tag{A4}$$

which produced results that compared well with experiment.

The expression for the angular velocity is simply

$$\Omega_t = \Omega_{t-\Delta t} + \dot{\Omega}_t(\Delta t) \tag{A5}$$

and the rate of descent becomes

$$V_{v_t} = V_{v_{t-\Delta t}} + \dot{V}_{v_t}(\Delta t) \tag{A6}$$

Hence, for a given model configuration and given variation of blade pitch angle, the minimum flare velocity may be determined by a step-by-step process.

It should be noted that the steady rate of vertical descent may be determined with good accuracy by the method of reference 4 with the exception that the rotor angular velocity must be determined by means of equation (A1) and the value of $1/f$ must be subsequently determined from the empirical curve of $1/f$ against $1/F$ of reference 2.

Sample calculation.- The physical properties for the helicopter chosen for the sample calculation are identical with those of the Bell Model 47 and are as follows:

$W = 2130$ lb

$b = 2$

$R = 17.55$ ft

$c_e = 0.91$ ft (effective chord)

$a = 5.75$ per radian

$c_{d_o} = 0.0088 + 0.30\bar{\alpha}^2$

$I_1 = 251$ lb-ft-sec^2 (slug-ft^2)

$\sigma = 0.033$

$\gamma_1 = 4.70$

The first step is to determine the vertical autorotation characteristics of the helicopter. The rotor autorotation angular velocity may be determined from equation (A1) for an assumed $\bar{\theta}_{auto} = 0^\circ$ since $\dot{V}_{v_{auto}} = 0$ and $\bar{C}_L = 0.297$ (fig. 17). Thus,

$$\Omega_{auto} = 42.9 \text{ radians/sec}$$

The rate of autorotative descent is then determined by the method of reference 4 with the exception that the value of $1/f$ is determined from the empirical curve of $1/f$ against $1/F$ of reference 2. Thus

$$V_{v_{auto}} = 32.3 \text{ ft/sec}$$

If it is also assumed that $t_\theta < 0.2$ second and if the Δt are taken in steps of 0.2 second, then both $\bar{C}_{L_t}$ and $\dot{\Omega}_t$ are constants throughout the flare maneuver. Therefore $\bar{\theta}_t = \bar{\theta}_f$ which is taken as 11° for this example. The following calculations may then be made:

$$\bar{C}_{L_{basic}} = 0.356 \qquad \text{(fig. 17)}$$

From equation (A3)

$$\Delta\bar{C}_L = 0.305$$

From equation (A2)

$$\bar{C}_L = 0.661 = \text{Constant}$$

From equation (A4)

$$\dot{\Omega} = -6.39 \text{ radians/sec}^2$$

From equation (A1)

$$\dot{V}_{v_t} = g - 0.0389\Omega_t^2$$

and Ω_t and V_{v_t} are determined from equations (A5) and (A6).

The results of this sample calculation are plotted as the curve labeled helicopter A in figure 21.

REFERENCES

1. Slaymaker, S. E., Lynn, Robert R., and Gray, Robin B.: Experimental Investigation of Transition of a Model Helicopter Rotor from Hovering to Vertical Autorotation. NACA TN 2648, 1952.

2. Castles, Walter, Jr., and Gray, Robin B.: Empirical Relation Between Induced Velocity, Thrust, and Rate of Descent of a Helicopter Rotor as Determined by Wind-Tunnel Tests on Four Model Rotors. NACA TN 2474, 1951.

3. Nikolsky, A. A., and Seckel, Edward: An Analysis of the Transition of a Helicopter from Hovering to Steady Autorotative Vertical Descent. NACA TN 1907, 1949.

4. Nikolsky, A. A., and Seckel, Edward: An Analytical Study of the Steady Vertical Descent in Autorotation of Single-Rotor Helicopters. NACA TN 1906, 1949.

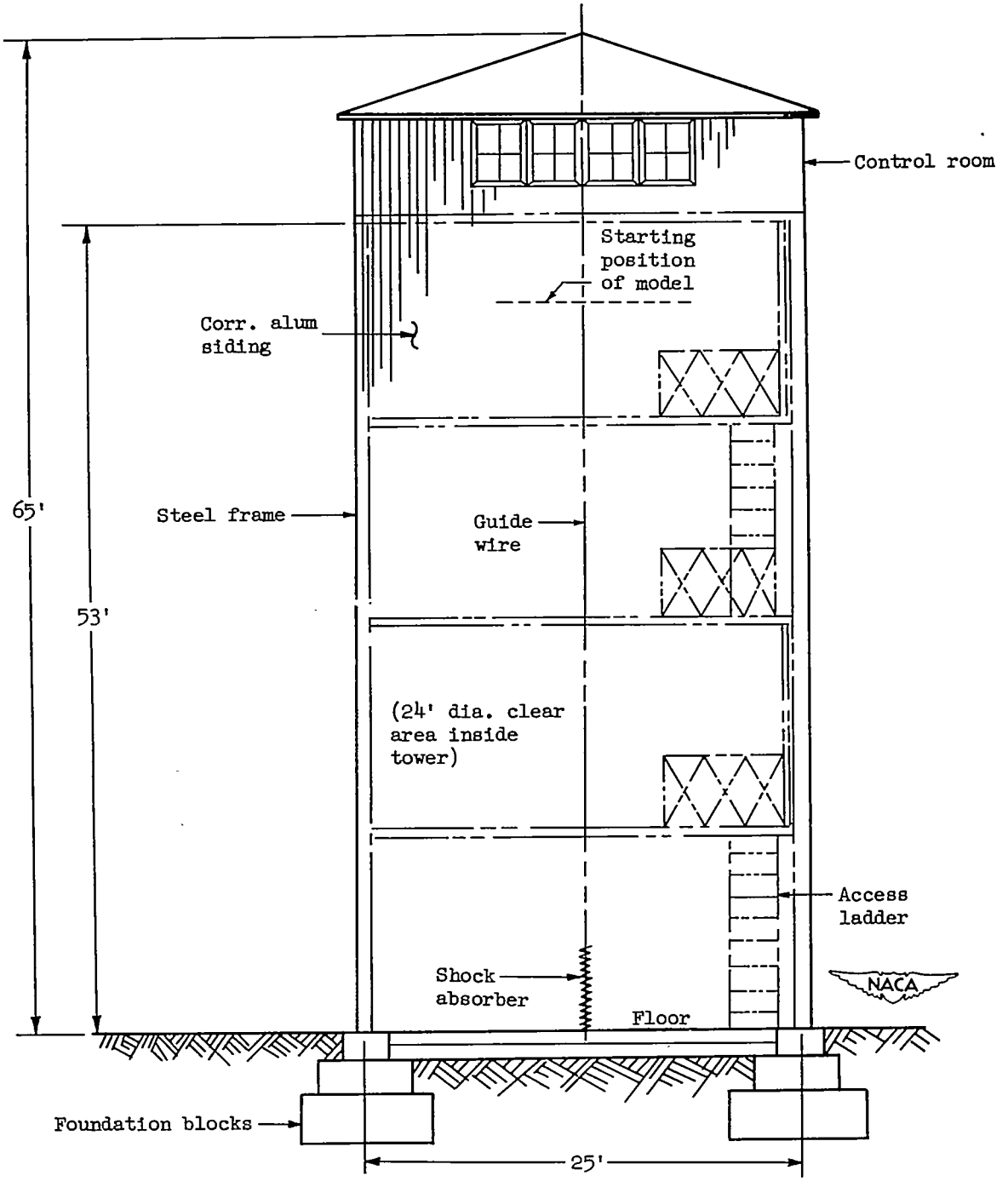

Figure 1.- Helicopter model research tower.

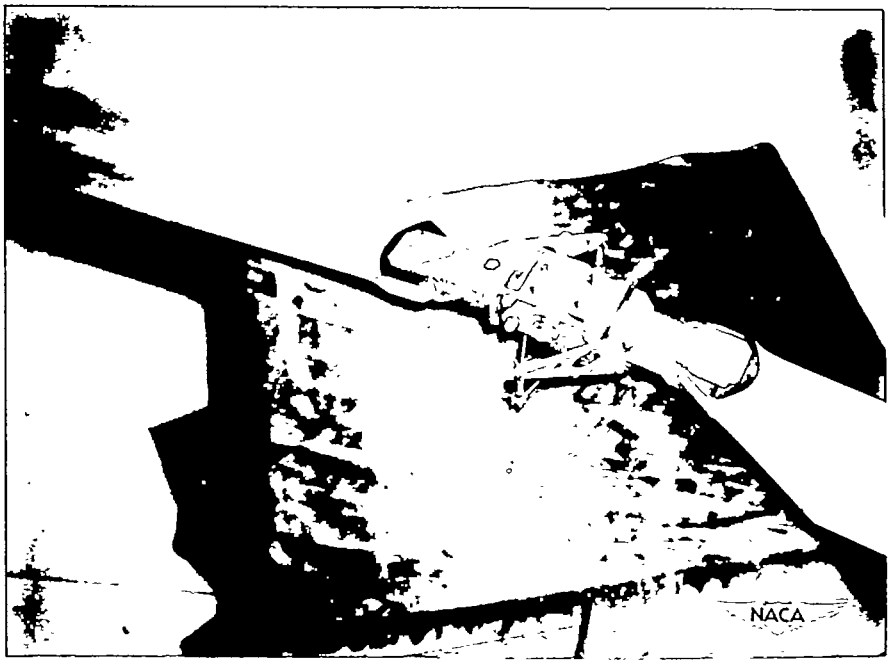

Figure 2.- Basic model rotor without pitch-control units or flash-bulb system.

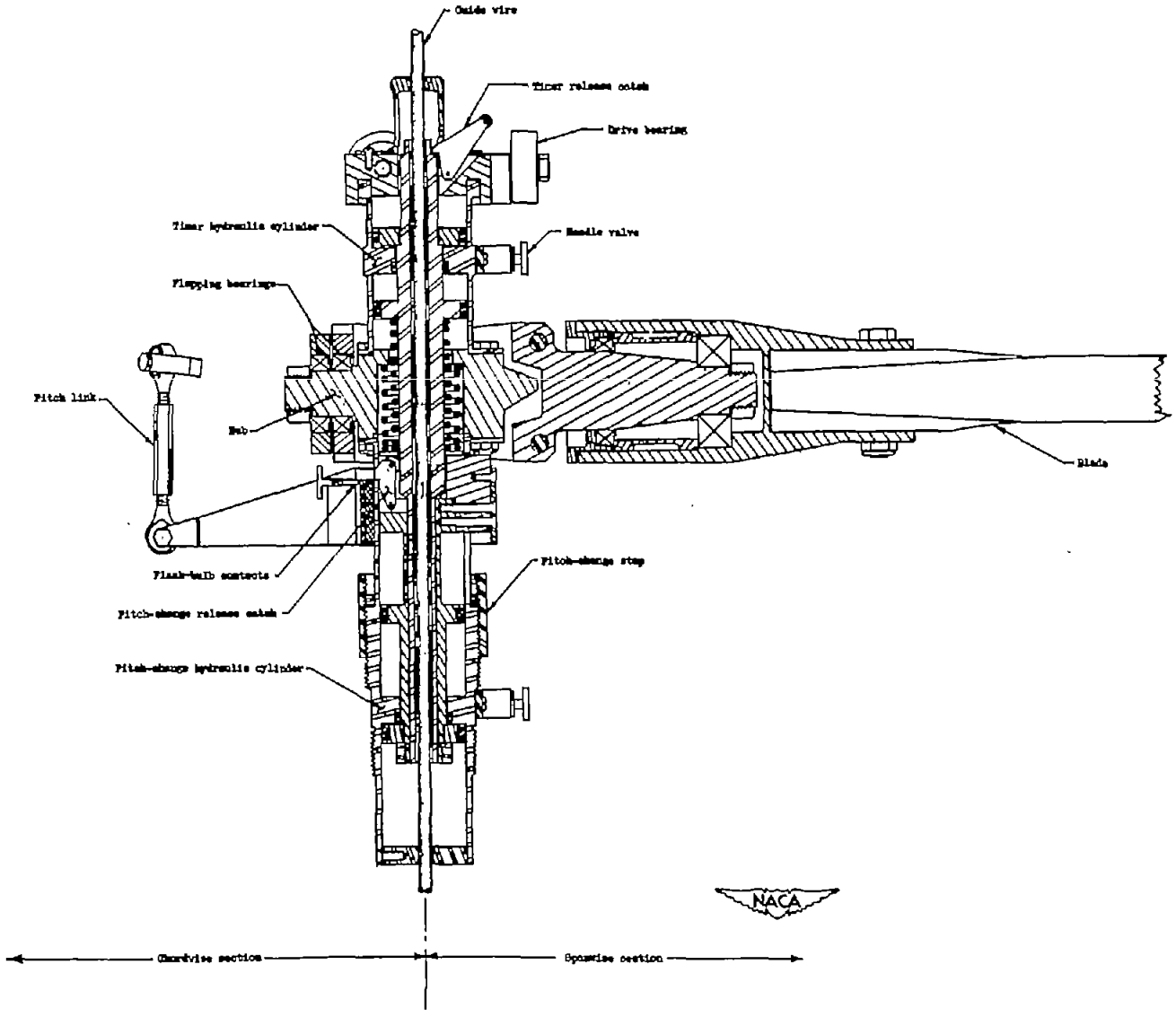

Figure 3.- Hub mechanism for helicopter model.

Figure 4.- Details of rotor hub, showing pitch-control cylinder and flash-bulb contacts. Flash bulbs are located inside black shields. Lead weight at bottom raises disk loading.

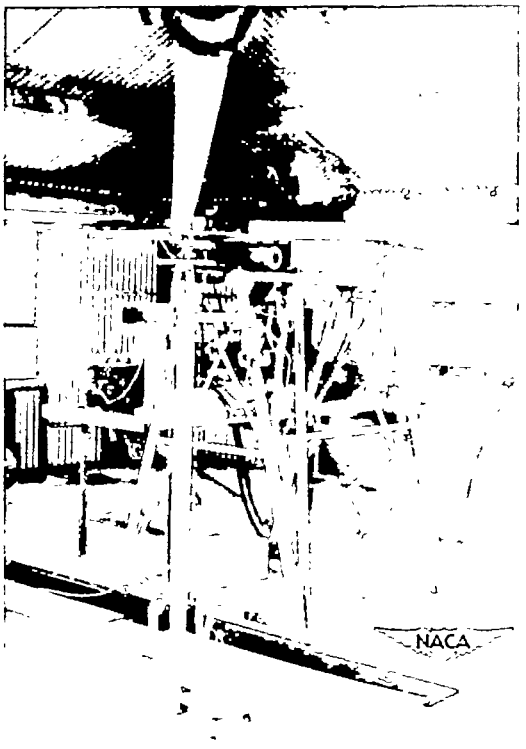

Figure 5.- Model drive system and controls. Note accelerating cords attached to drive shaft.

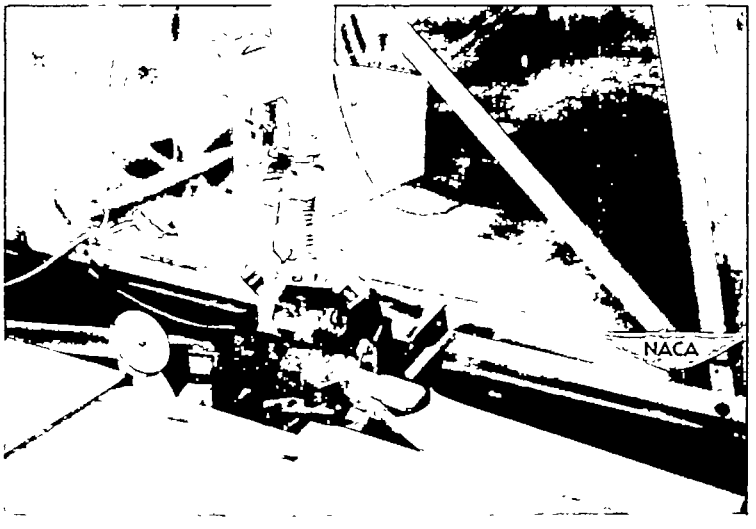

Figure 6.- Details of release mechanism on drive shaft.

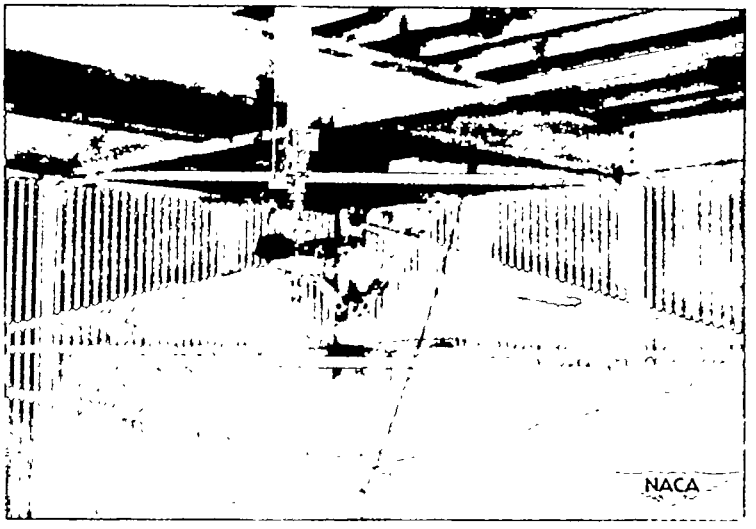

Figure 7.- Model connected to drive shaft in starting position.

Figure 8.- Drive shaft in final position at end of acceleration stroke.

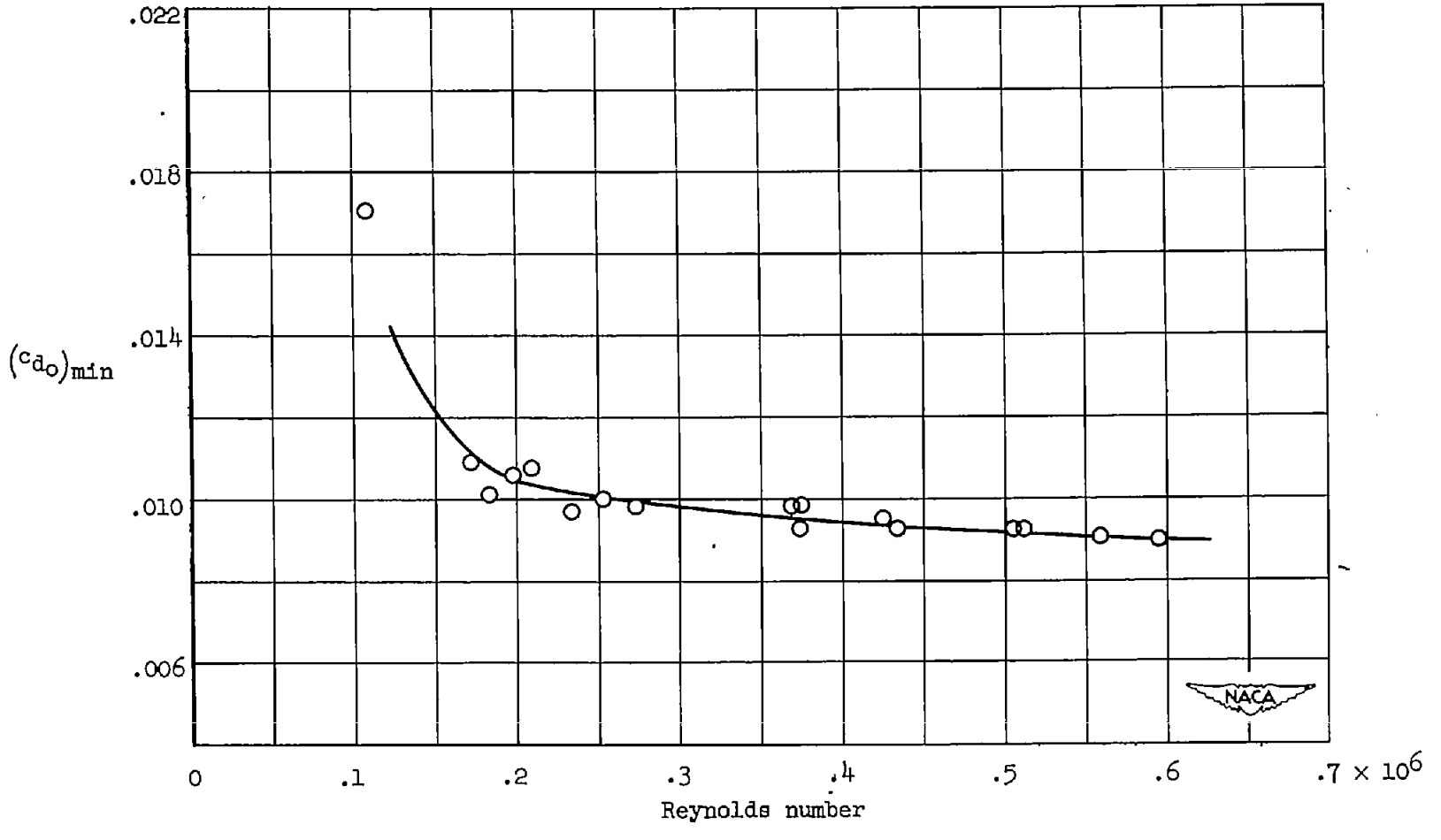

Figure 9.- Minimum profile-drag coefficient against Reynolds number.

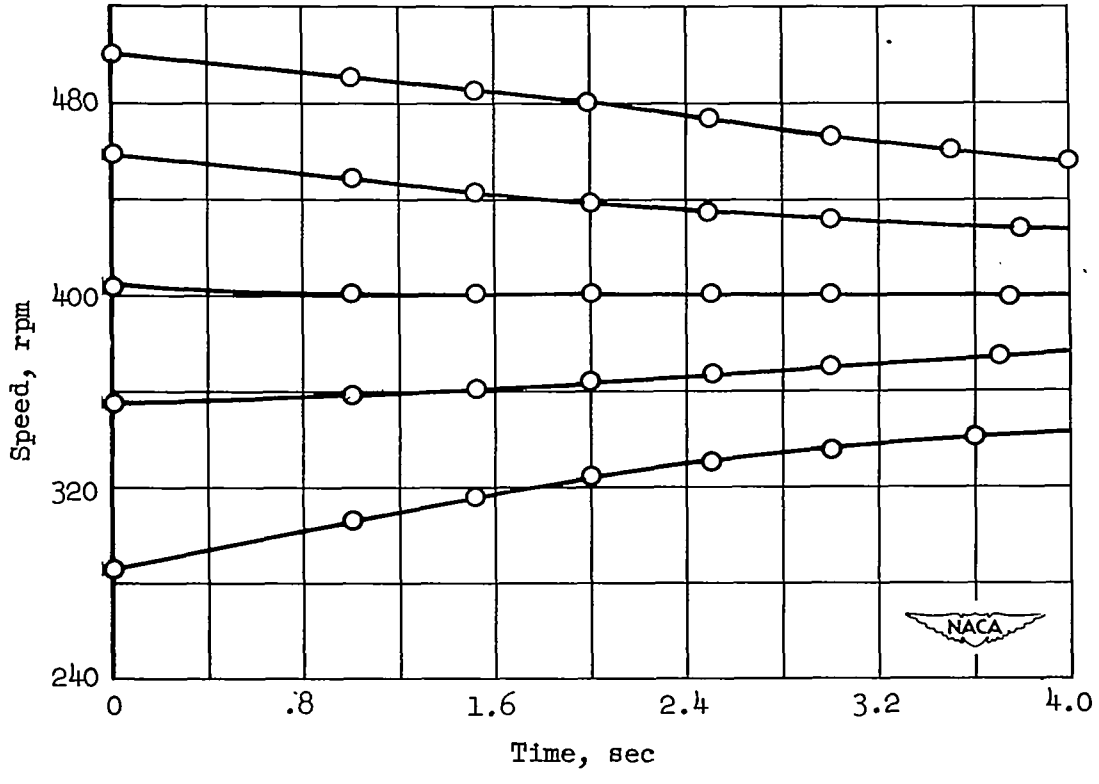

Figure 10.- Determination of autorotative speed. W/S = 0.246 pound per square foot; $\overline{\theta}_0 = 0^\circ$.

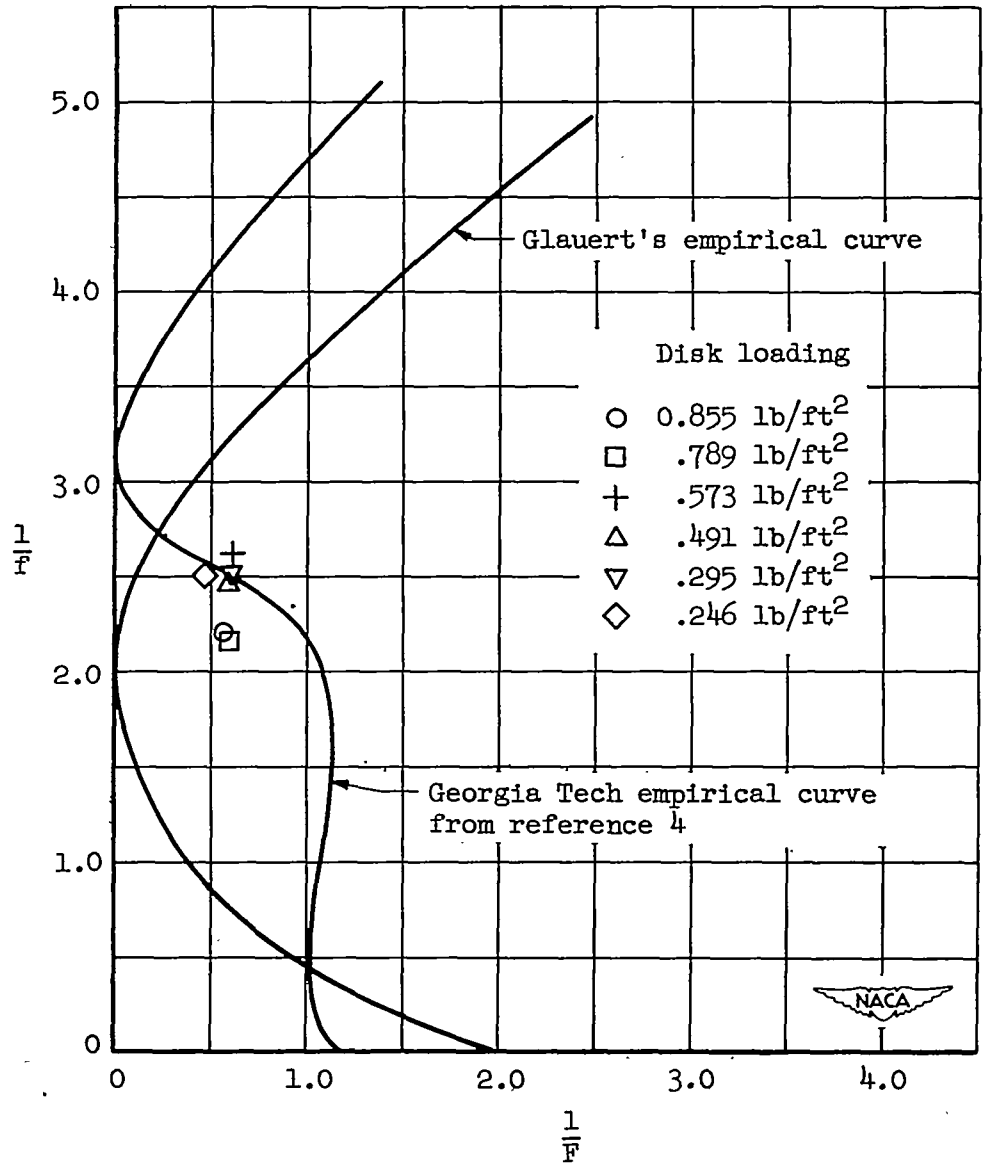

Figure 11.- Plot of autorotative-descent data of a model helicopter on 1/f against 1/F coordinates.

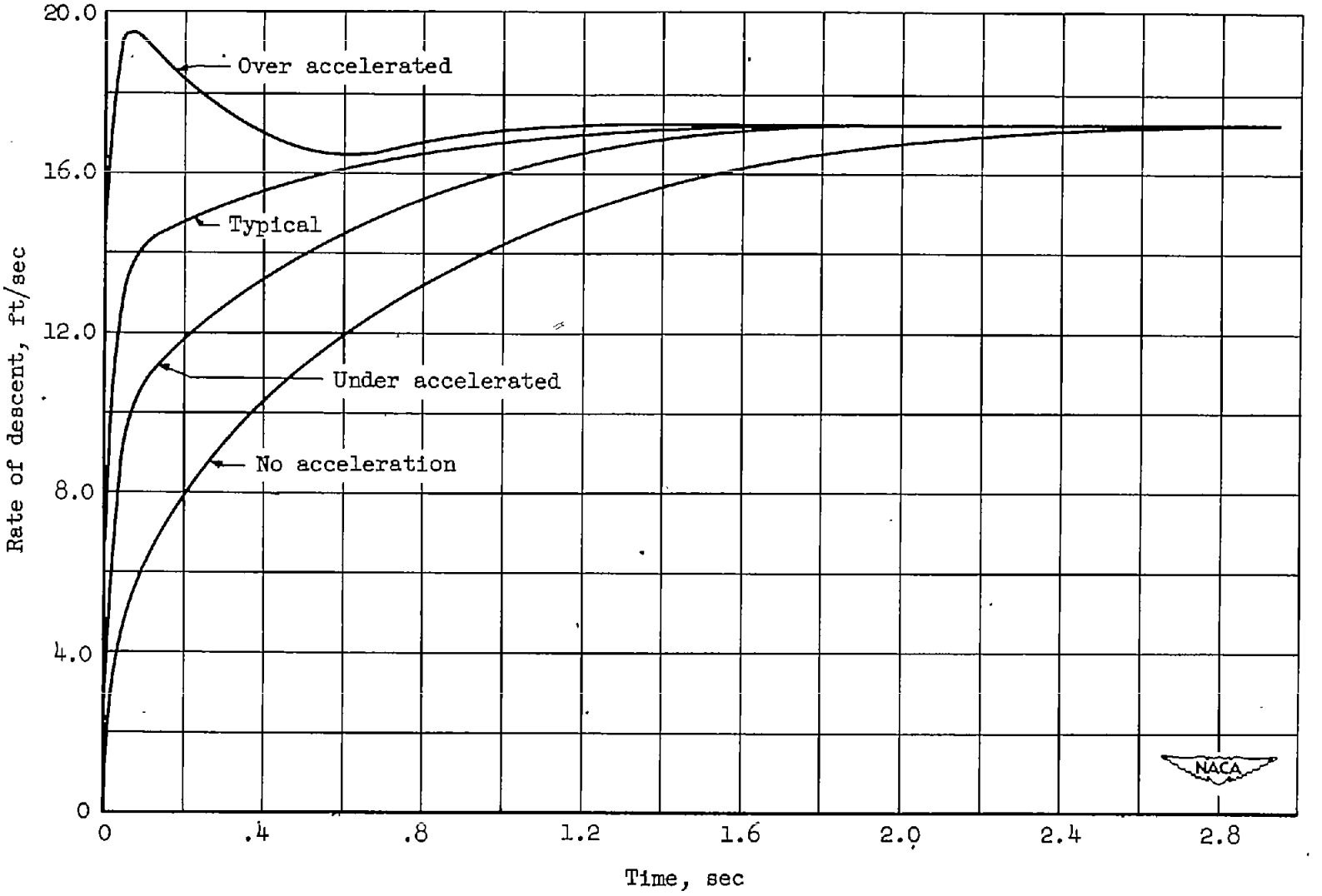

Figure 12.- Effect of initial acceleration on descending velocity. W/S = 0.491 pound per square foot; $\overline{\theta}_o = 0^o$.

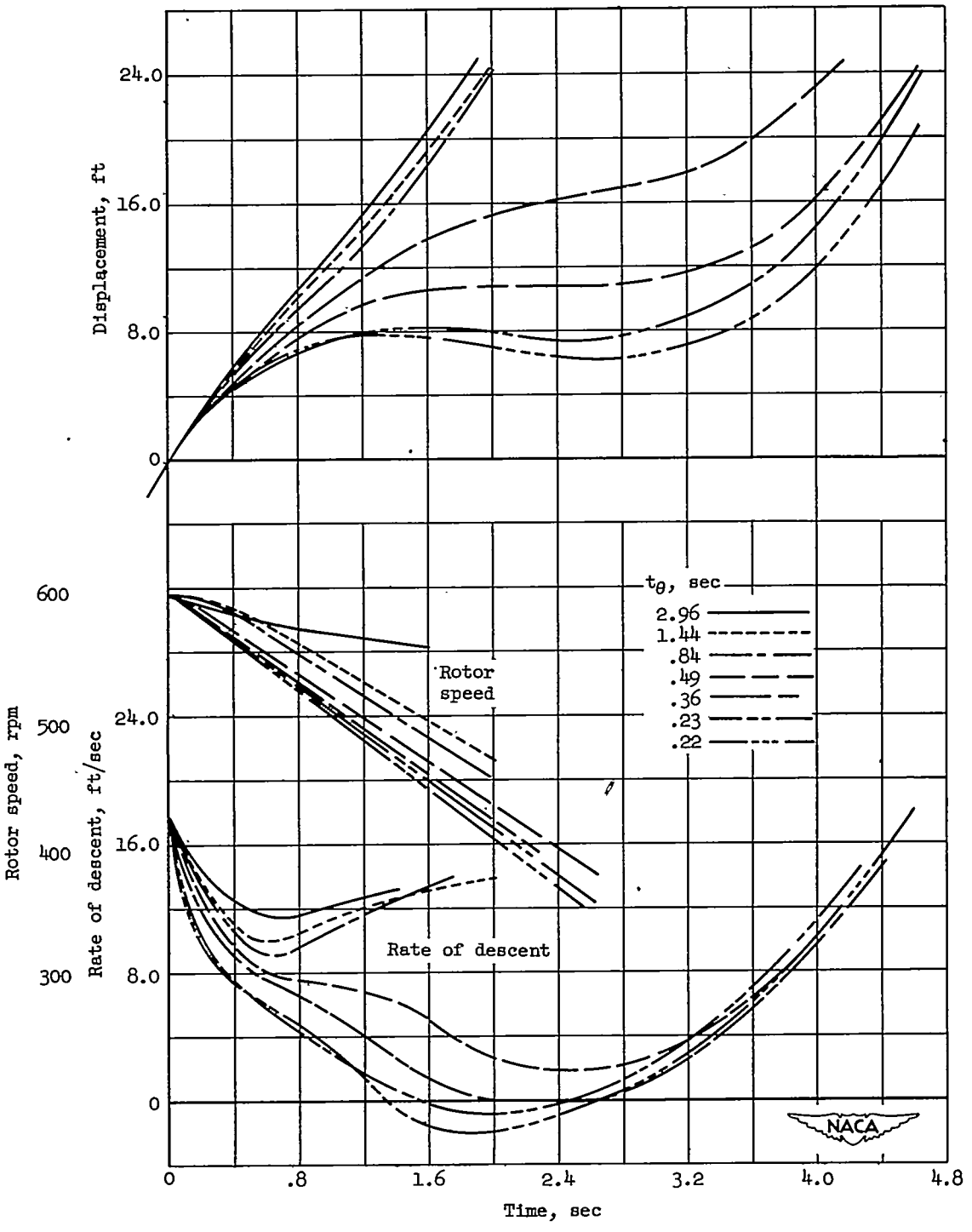

Figure 13.- Effect of total pitch-change time on displacement, rate of descent, and speed of a model helicopter rotor. W/S = 0.573 pound per square foot; $\overline{\theta}_f = 12\frac{1}{2}^\circ$; $\gamma_1 = 2.8$.

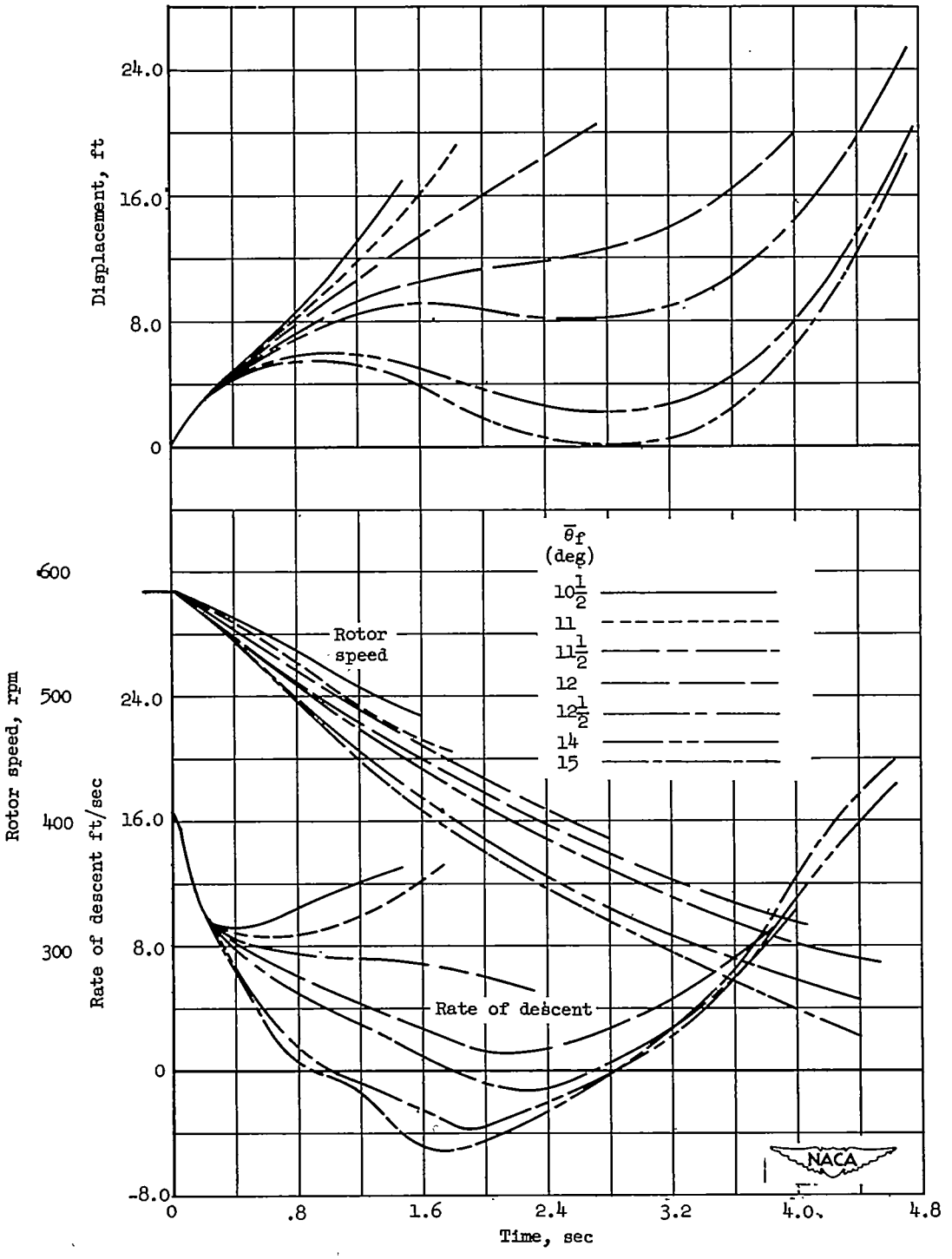

Figure 14.- Effect of final blade pitch angle on displacement, rate of descent, and speed of a model helicopter rotor. W/S = 0.573 pound per square foot; $t_{\bar{\theta}} = 0.99\theta_f^{1.20}$; $\gamma_1 = 2.8$.

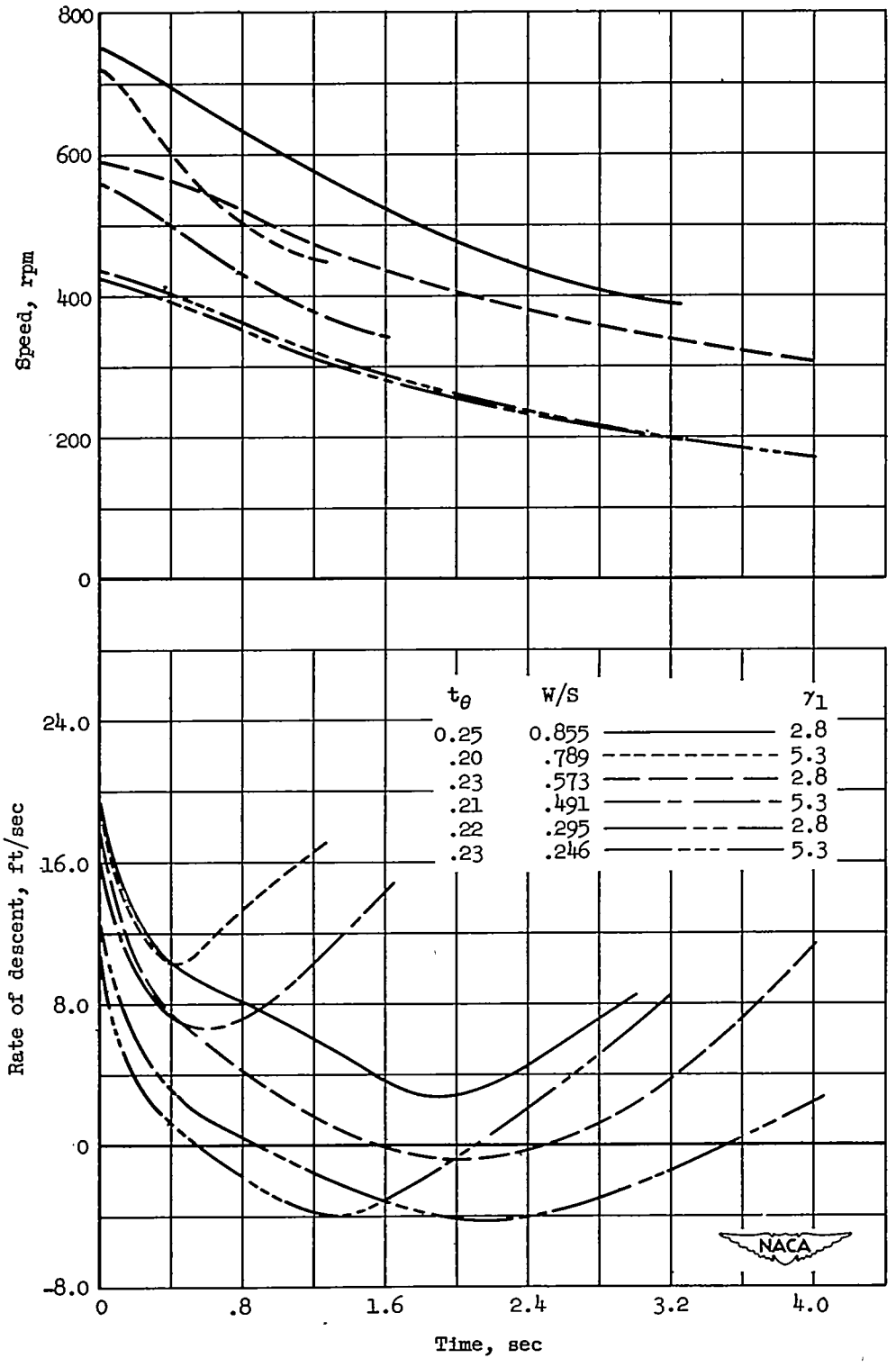

Figure 15.- Effect of rotor inertia and disk loading on speed and rate of descent of a model helicopter rotor. $\overline{\theta}_o = 0^\circ$; $\overline{\theta}_f = 12\frac{1}{2}^\circ$.

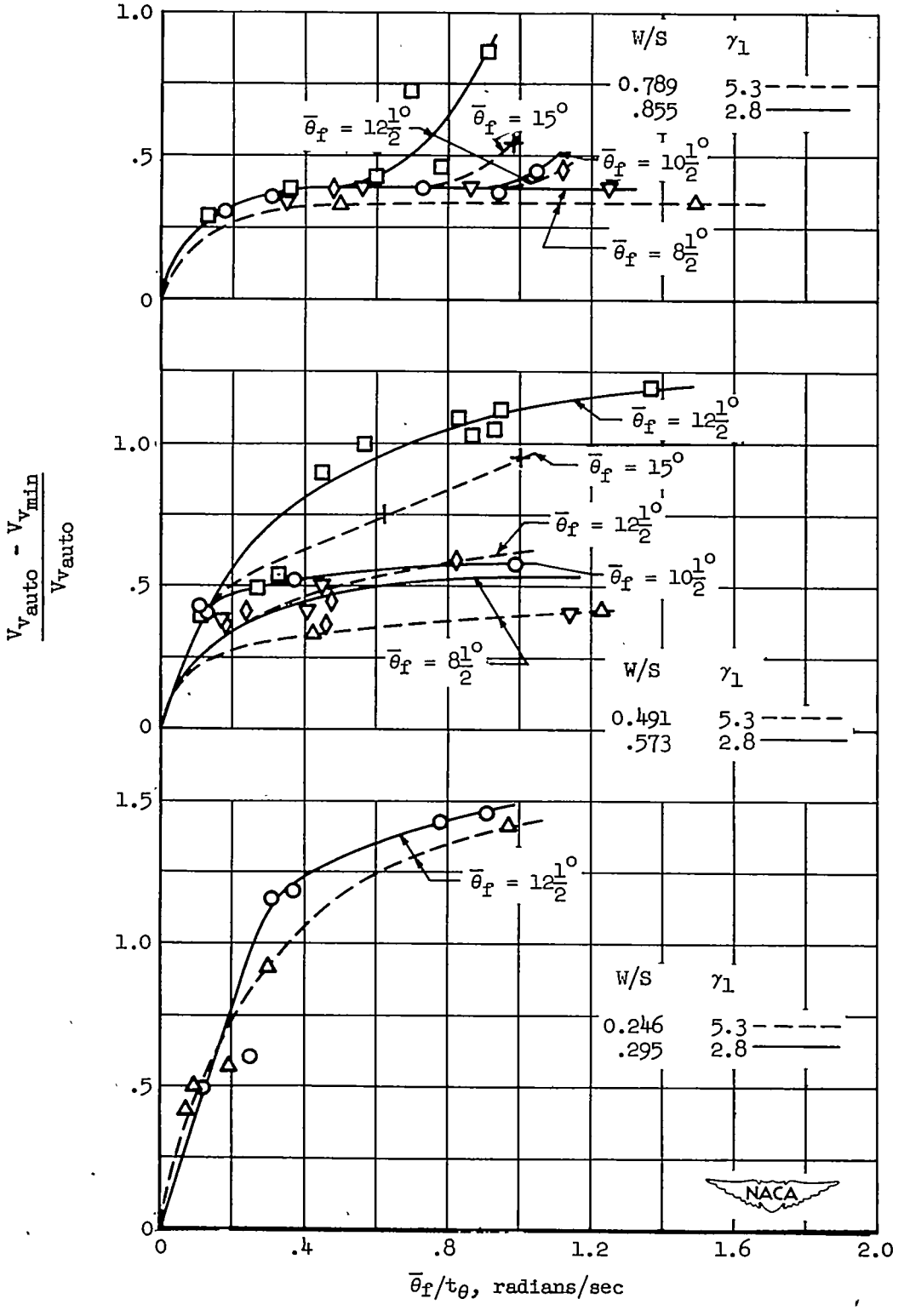

Figure 16.- Effect of average rate of blade pitch change on change in rate of descent during flare-up of model helicopter rotor. $\bar{\theta}_o = 0^\circ$.

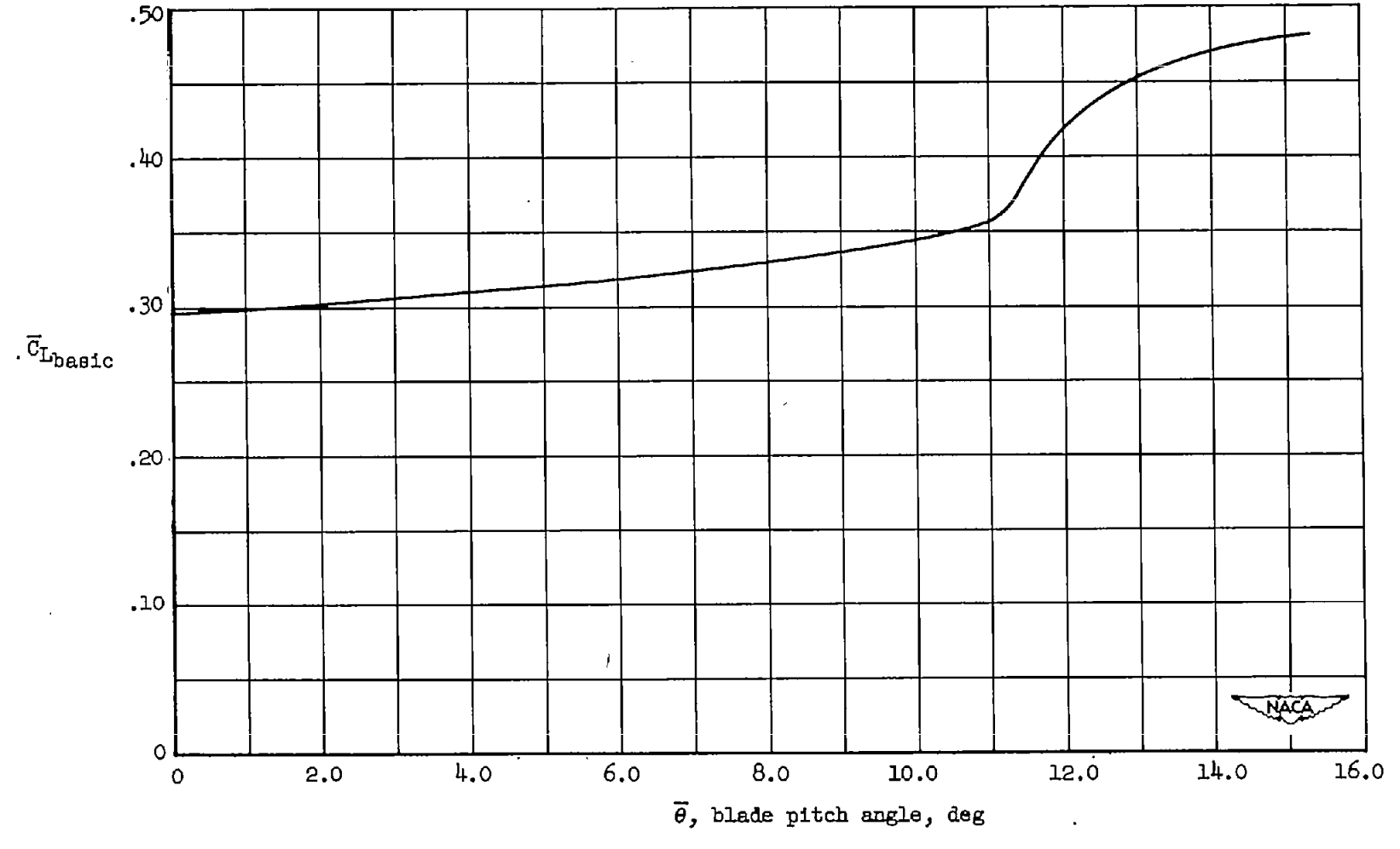

Figure 17.- Variation of average basic rotor lift coefficient with blade pitch angle during flare-up from steady vertical autorotation for a model helicopter.

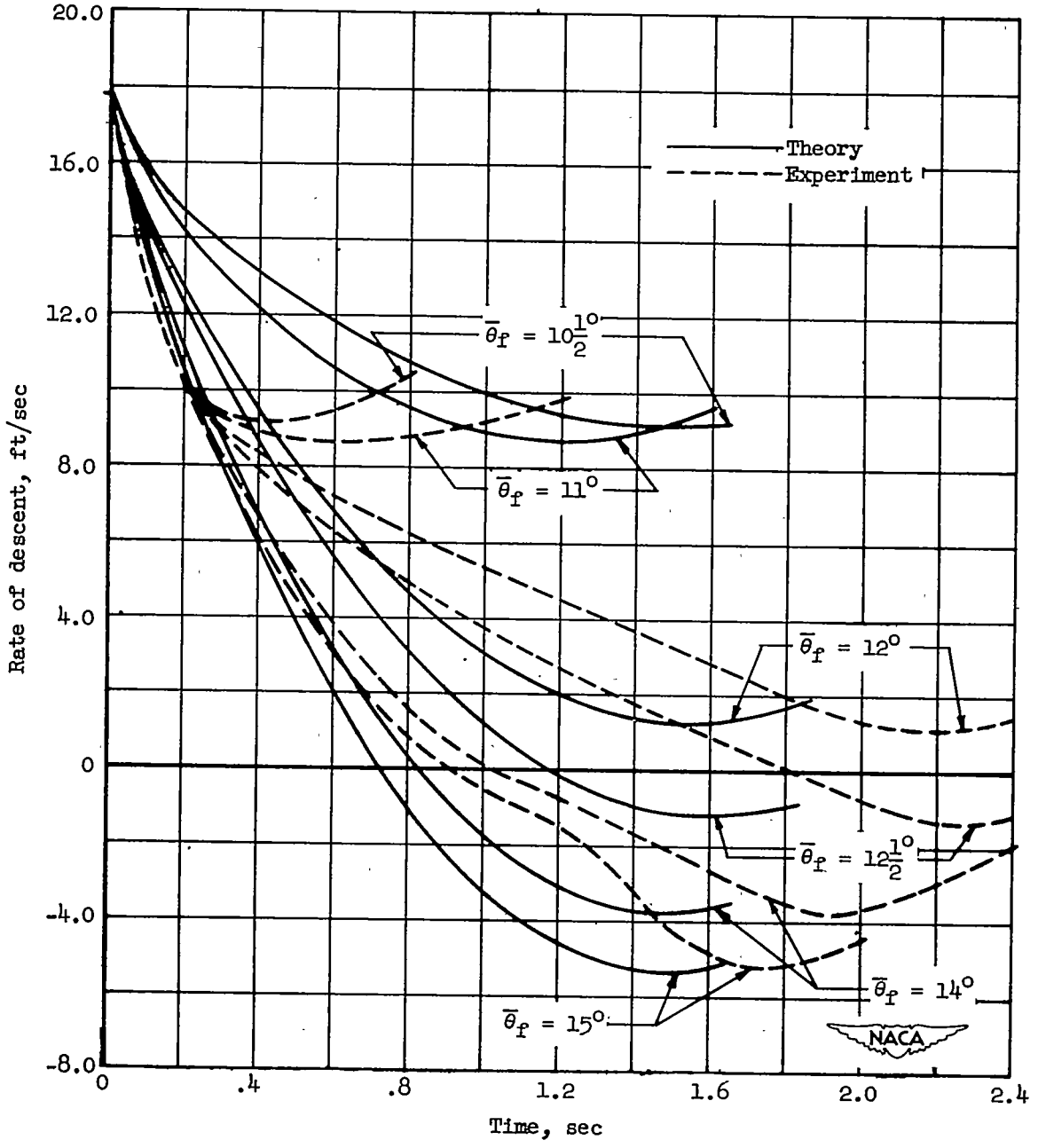

Figure 18.- Comparison of semiempirical theory with experiment for flare-ups from steady vertical autorotation for a model helicopter rotor. W/S = 0.573 pound per square foot; $\sigma = 0.0796$; $I_R = 1.25$ pound-feet-second^2; R = 4 feet; $t_\theta = 0.2$ second; $\bar{\theta}_o = 0^\circ$; $\gamma_1 = 2.8$.

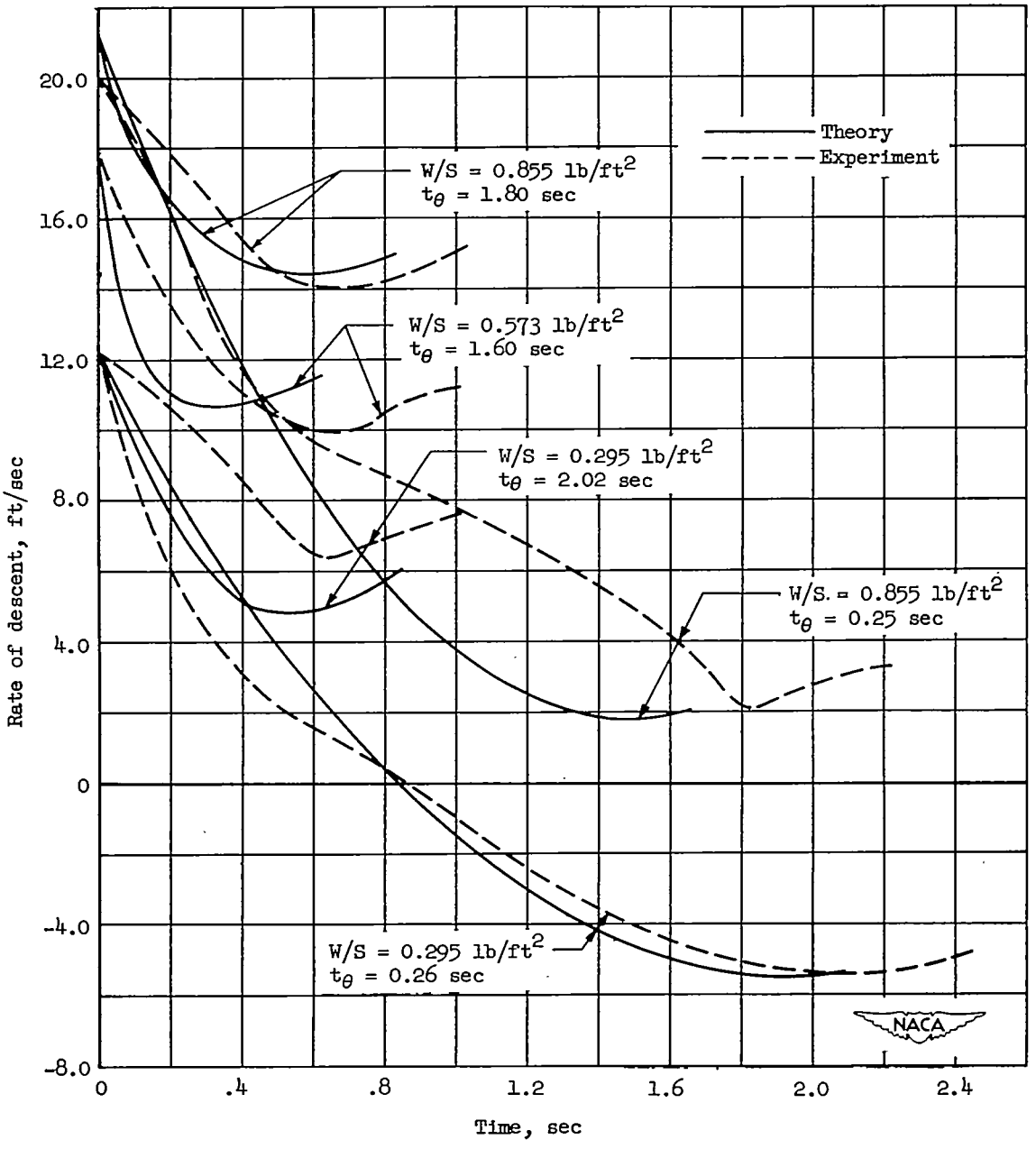

Figure 19.- Comparison of semiempirical theory with experiment for flare-ups from steady vertical autorotation for a model helicopter rotor. σ = 0.0796; I_R = 1.25 pound-feet-second^2; R = 4 feet; $\overline{\theta}_o = 0^\circ$; $\overline{\theta}_f = 12\frac{1}{2}^\circ$; γ_1 = 2.8.

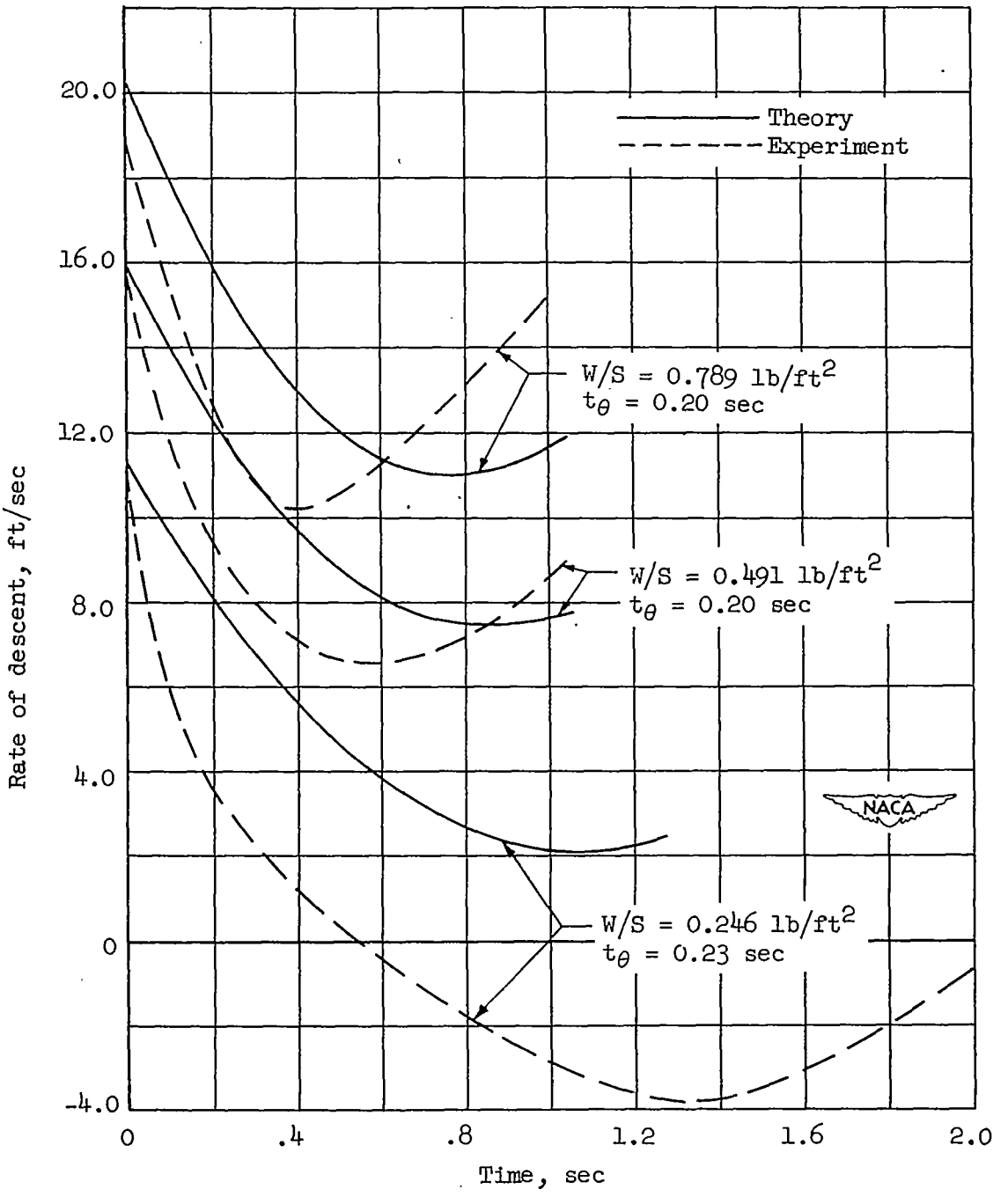

Figure 20.- Comparison of semiempirical theory with experiment for flare-ups from steady vertical autorotation for a model helicopter rotor. σ = 0.0796; I_R = 0.66 pound-feet-second^2; R = 4 feet; $\overline{\theta}_o = 0^o$; $\overline{\theta}_f = 12\frac{1}{2}^o$; γ_1 = 5.3.

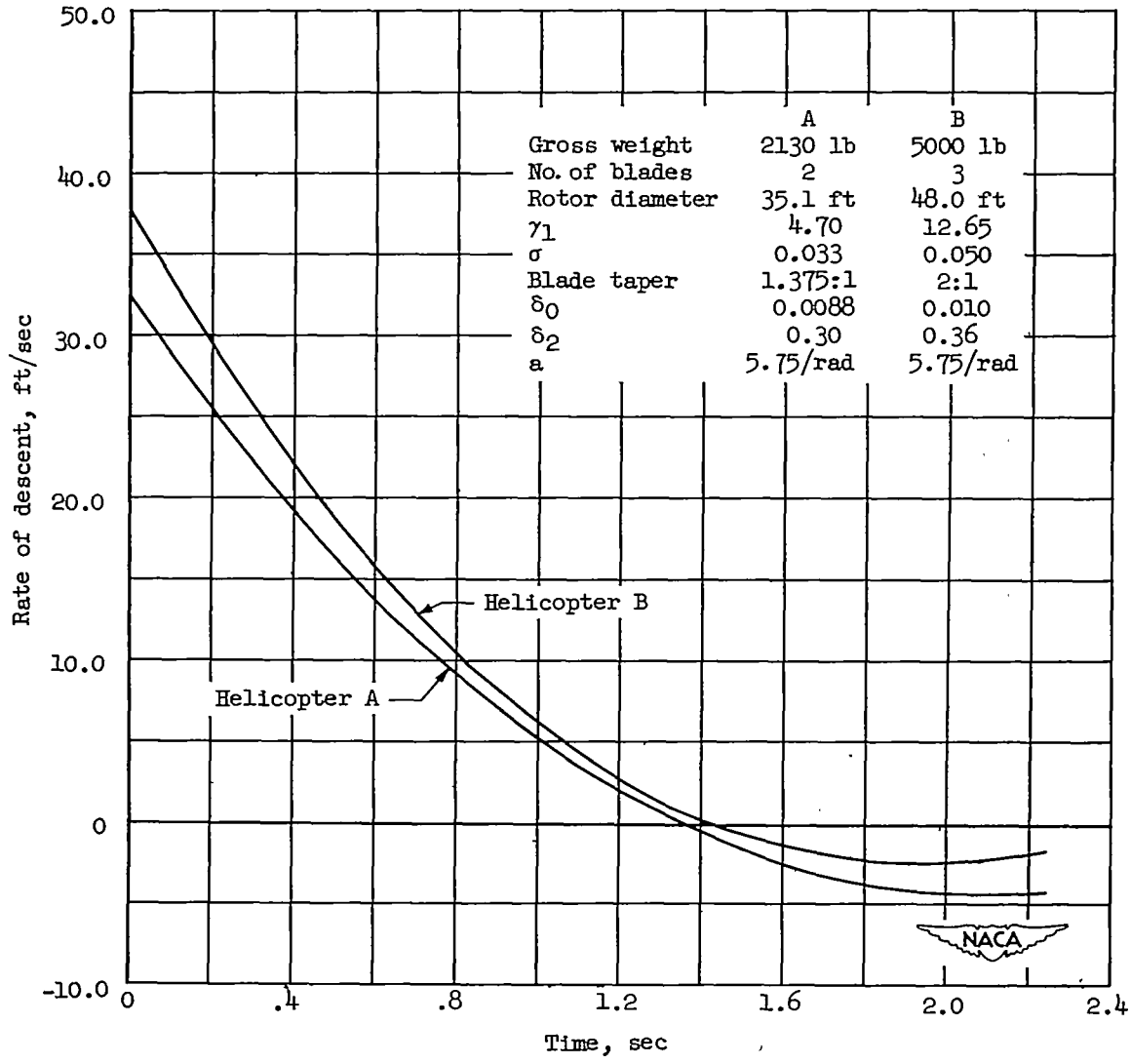

Figure 21.- Flare-up performance of two full-scale helicopters in vertical autorotation as predicted by semiempirical theory. $\overline{\theta}_o = 0^\circ$; $\overline{\theta}_f = 11^\circ$; $t_\theta = 0.2$ second. Power requirements of countertorque rotor and effect of fuselage not included.

NACA-Langley - 1-16-53 - 1000